

A residual based error estimator using radial basis functions

Bernard B.T. Kee^{a,*}, G.R. Liu^{a,b}, G.Y. Zhang^{a,b}, C. Lu^c

^aCentre for Advanced Computations in Engineering Science (ACES), Department of Mechanical Engineering, National University of Singapore, 9 Engineering Drive 1, Singapore 117576, Singapore

^bThe Singapore-MIT Alliance (SMA), E4-04-10, 4 Engineering Drive 3, Singapore 117576, Singapore

^cInstitute of High Performance Computing (IHPC), 1 Science Park II, Singapore 117528, Singapore

Received 16 January 2007; received in revised form 11 December 2007; accepted 24 February 2008

Available online 6 May 2008

Abstract

In this paper, a novel residual based error estimator using radial basis functions (RBFs) is proposed. The error estimator evaluates the residual in the strong-form governing equation in the local domain through direct integration. Due to the higher order continuous feature of the RBFs, the higher derivatives of the field function in the strong-form governing equation can be obtained using RBFs. The numerical examples show that the new residual based error estimator is simple, versatile robust and yet effective in the adaptive analyses. It is not only suitable for adaptive analysis that uses numerical method formulated based on mesh, e.g. finite element method, but also meshfree methods where the conventional residual based and recovery based error estimator cannot be used. Furthermore the present error estimator is also feasible for numerical method that is formulated based on both strong and weak formulation in the adaptive analyses.

© 2008 Elsevier B.V. All rights reserved.

Keywords: Error estimator; Radial basis functions; Adaptive; Residual; Finite element method; Meshfree method

1. Introduction

Adaptive analysis is an important study in the computational mechanics and engineering. Numerous research works have been conducted in the area of adaptive analysis in the past few decades. The ultimate goal of the adaptive analysis is to obtain numerical solution with desired accuracy through adaptive analysis process with minimum computation cost. Through an effective refinement scheme, the discretization error can be reduced by refining the region in the problem domain where the accuracy of the numerical solution is low, and hence achieve the prescribed accuracy. Therefore, a robust and effective error estimator plays a very crucial role to identify the quality of the numerical solution. Without a reliable error estimator, a good adaptive analysis can never be performed effectively.

In general, error estimator can be classified into two major types, which are recovery based and residual based error estimators. The recovery based error estimator is first introduced by Zienkiewicz and Zhu in 1987 [1]. This error estimator is obtained through the recovery processes and always expressed in terms of the energy norm. Many recovery based error estimators have been reported after then [2–4]. Zienkiewicz et al. have also published a series of intensive works that is devoted to the recovery based error estimator [5–7].

Residual based error estimators have been proposed much earlier than recovery based error estimator. In 1978, residual based error estimator was first introduced by Babuska and Rheinboldt [8]. Many works related to the residual based error estimator have been published, for examples, the residual equilibration by Ainsworth and Oden [9].

In this paper, a residual based error estimator using radial basis functions (RBFs) is present. The residual in the strong-form governing equation is evaluated in the local domain to reflect the quality of the numerical solution locally. The measure of residual is evaluated through direct integration. As RBFs possess higher order of continuity, the higher derivatives of the field function involved in the strong-form governing equation

* Corresponding author. Tel.: +65 65164797.

E-mail addresses: g0301110@nus.edu.sg (B.B.T. Kee), mpeliugr@nus.edu.sg (G.R. Liu), g0203729@nus.edu.sg (G.Y. Zhang), luchun@ihpc.a-star.edu.sg (C. Lu).

can be approximated. RBFs are well-known for its excellence performance in curve fitting and interpolation [10,11]. In the early 1990s, Kansa had also extended the RBFs to solve the partial differential equations (PDEs) [12,13]. Recently, many meshfree methods using RBFs to construct their shape function for field function approximation. Liu et al. have reported a series of research works that adopted RBFs for function approximation using local nodes [14–18]. In this paper, as RBFs possess higher order of continuity, it can be used to obtain the higher derivatives of the field function that are required for the direct integration of the residual in the strong-form equation and local domain. Whereas, the continuity of polynomial function is very much restricted by the order of basis, obtaining higher derivatives may not be achievable.

This works will demonstrate the following advantages of residual based error estimator using RBFs:

1. The formulation of the present estimator is simple and straightforward. The computational cost of the present formulation is lower than the conventional residual based error estimator.
2. The implementation of the present estimator is rather simple. It is very convenient to embrace the present error estimator with existing codes of any numerical method, e.g. finite element method (FEM).
3. RBFs are very robust to approximate the higher derivatives of the field function using scattered nodes. In contrast, the approximation that uses polynomials function is often breakdown due to the singular moment matrix [14,19].
4. Unlike the recovery based error estimator, the present error estimator does no involve recovery process. The cost for

However, at the current stage of this work, the residual based error based error estimator is restricted to linear problems only. The present error estimator is also feasible for heterogeneous materials where discontinuity stress functions exist across the interface of different materials. Although no nonlinear problem, for example, elasto-plastics problem, is studied in this work, many problems with high gradient solution and singularity points are presented.

2. Approximation function

RBFs are well known and have been widely used for interpolation and curve fitting [10,11]. In this work, RBFs augmented with monomial terms are used here as a function approximation to approximate the field function. Many types of RBFs with arbitrary shape parameters are available as given in Table 1 [21,22].

An unknown field function u can be approximated at any interest point \mathbf{x} by local radial point interpolation in the following form as

$$u^h(\mathbf{x}) = \sum_{i=1}^n a_i r_i(\|\mathbf{x} - \mathbf{x}_i\|) + \sum_{j=1}^m b_j p_j, \tag{1}$$

where n is the total number of the supporting nodes in the local domain, m is the number of monomials in the polynomial function, $r_i(\|\cdot\|)$ is the RBF and p_j is the monomial in polynomial function for augmentation. a_i and b_j are the coefficient of RBF and monomial of polynomial function.

Enforcing the local radial point interpolation to pass through the nodal value at the supporting nodes in the local domain, we have

$$\begin{bmatrix} u_1 \\ u_2 \\ \vdots \\ u_n \end{bmatrix} = \begin{bmatrix} r_1(\|\mathbf{x}_1 - \mathbf{x}_1\|) & r_1(\|\mathbf{x}_1 - \mathbf{x}_2\|) & \cdots & r_1(\|\mathbf{x}_1 - \mathbf{x}_n\|) & p_1(\mathbf{x}_1) & \cdots & p_m(\mathbf{x}_1) \\ r_2(\|\mathbf{x}_2 - \mathbf{x}_1\|) & r_2(\|\mathbf{x}_2 - \mathbf{x}_2\|) & \cdots & r_2(\|\mathbf{x}_2 - \mathbf{x}_n\|) & p_1(\mathbf{x}_2) & \cdots & p_m(\mathbf{x}_2) \\ \vdots & \vdots & \ddots & \vdots & \vdots & \ddots & \vdots \\ r_n(\|\mathbf{x}_n - \mathbf{x}_1\|) & r_n(\|\mathbf{x}_n - \mathbf{x}_2\|) & \cdots & r_n(\|\mathbf{x}_n - \mathbf{x}_n\|) & p_1(\mathbf{x}_n) & \cdots & p_m(\mathbf{x}_n) \end{bmatrix} \begin{bmatrix} a_1 \\ \vdots \\ a_n \\ b_1 \\ \vdots \\ b_m \end{bmatrix} \tag{2}$$

recovery process is therefore avoided although this is minor as compared to the entire computational cost.

5. Compared to recovery based error estimator, the knowledge for recovery point is not required. For meshfree method, obtaining recovery points may not be feasible.
6. As conventional residual based error estimator is involved in evaluating the traction jump of the element interface [20], it is not applicable for some meshfree methods where the element does not exist in their formulation procedure.
7. This error estimator can be applied for solving various types of PDEs. It is not restricted to particular problems only.
8. It is obvious that the present error estimator is very versatile. It is not only feasible for numerical method that formulated relying on mesh, for instance, FEM, but also the meshfree methods. It is also suitable for both weak and strong formulation procedure as well.
9. From the numerous numerical examples, the error estimator is shown robust, effective, reliable, versatile and simple.

or

$$\mathbf{U} = [\mathbf{R} \quad \mathbf{P}] \begin{bmatrix} \mathbf{a} \\ \mathbf{b} \end{bmatrix},$$

where \mathbf{U} is the vector of unknown nodal values, \mathbf{a} and \mathbf{b} are the vectors of coefficients for RBFs and monomials of the polynomial function, respectively.

Table 1
Typical generalized radial basis functions [21,22], where $r_i = \|\mathbf{x} - \mathbf{x}_i\|$ is the Euclidian norm in the vector space

Type	Expression	Dimensionless parameter
Multiquadrics (MQ)	$R_i(x, y) = (r_i^2 + (\alpha_c d_c)^2)^q$	α_c, q
Gaussian (EXP)	$R_i(x, y) = \exp(-cr_i^2)$	c
Thin plate spline (TPS)	$R_i(x, y) = r_i^\eta$	η
Logarithmic	$R_i(x, y) = r_i^\eta \log r_i$	η

With orthogonal condition [23,13],

$$\mathbf{P}^T \mathbf{a} = \mathbf{0}, \tag{3}$$

the above Eqs. (2) and (3) can be combined as the following form as

$$\begin{Bmatrix} \mathbf{U} \\ \mathbf{0} \end{Bmatrix} = \begin{bmatrix} \mathbf{R} & \mathbf{P} \\ \mathbf{P}^T & \mathbf{0} \end{bmatrix} \begin{bmatrix} \mathbf{a} \\ \mathbf{b} \end{bmatrix} = \mathbf{G} \begin{bmatrix} \mathbf{a} \\ \mathbf{b} \end{bmatrix}. \tag{4}$$

Hence, the vector of coefficients can be obtained as

$$\begin{bmatrix} \mathbf{a} \\ \mathbf{b} \end{bmatrix} = \mathbf{G}^{-1} \begin{Bmatrix} \mathbf{U} \\ \mathbf{0} \end{Bmatrix}. \tag{5}$$

The approximated field function $u^h(\mathbf{x})$ can be then expressed in the following form as

$$u^h(\mathbf{x}) = [\phi_1(\mathbf{x}) \quad \phi_2(\mathbf{x}) \quad \cdots \quad \phi_n(\mathbf{x})] \mathbf{U} = \Phi(\mathbf{x})\mathbf{U}, \tag{6}$$

where $\phi_i(\mathbf{x})$ is the shape function (RPIM shape function) for supporting node i .

The derivatives of the field function can also be easily expressed using RPIM shape function. For instance, the first derivative of the field function u respect to k can be given as

$$u_{,k}^h(\mathbf{x}) = [\phi_{1,k}(\mathbf{x}) \quad \phi_{2,k}(\mathbf{x}) \quad \cdots \quad \phi_{n,k}(\mathbf{x})] \mathbf{U} = \Phi_{,k}(\mathbf{x})\mathbf{U}, \tag{7}$$

where $\phi_{i,k}(\mathbf{x})$ is the first derivative of the shape function respect to k for supporting node i .

The details of RPIM shape function property are well discussed in the [21,22]. Due to the editorial limitation, it is very difficult to present various types of RBF in one paper. Therefore, only the well-known multiquadrics (MQ) RBF is used in this paper. As other RBFs also demonstrate excellence performance in curve fitting and interpolation, we believe that other RBFs can achieve similar results that MQ-RBF can obtain. In this work, MQ-RBF augmented with completed second order polynomial function is used in the function approximation. The shape parameters used for MQ is adopted from the recommended values reported by Liu et al. [16,21,22]: $\alpha_c = 3.0$ and $q = 1.03$.

3. Error estimate

In this work, we propose an error estimator that is formulated based on the residual in the strong-form governing equation. This residual based error estimator provides some physical interpretation. The measure is an indicator of the equilibration in the local domain. The quality of the approximated solution can therefore be reflected in this measure.

Consider a system governed by the PDE as

$$L(u) + f = 0 \quad \text{in the problem domain } \Omega \tag{8}$$

where $L(\cdot)$ is a differential operator and u is the field function in the domain. The present residual based error estimator is defined as

$$\eta_L := \int_{\Omega^T} Res^T d\Omega, \tag{9}$$

where Ω^T denotes the local domain and Res^T is the residual in the strong-form governing equation that measured in the

local domain Ω^T by the numerical solution u^h . The residual is defined as follows:

$$Res^T := \|L(u^h) + f\|_{L_2}. \tag{10}$$

This error estimator represents the equilibration of the local domain in the form of scalar L2 norm. In the numerical integration scheme for evaluation of the residual in the local domain, one point gauss integration scheme is used. Thus, the local error estimator can further simplified as

$$\eta_L = Res^T \times |T|, \tag{11}$$

where $|T|$ is the area of the local domain. Furthermore, the estimated global residual norms is defined as

$$\eta_G = \int_{\Omega} \|Res^T\|_{L_2} d\Omega, \tag{12}$$

which is the L2 norm of the residual in the entire problem domain.

Note that the higher derivative of the differential operator can be approximated using RBF interpolation. Compared to the conventional residual based error estimator that measures the traction jump along the interface of the element [20], the cost of measuring the residual that using direct integration is much cheaper. Furthermore, measuring traction jump is not feasible for meshfree method.

4. Adaptive strategy

In this work, a simple h -refinement scheme is adopted. The problem domain is first discretized using Delaunay diagram. The present error estimator is then measured for each individual cell. The local domain will be refined if the refinement criteria is met. The refinement criteria is defined as

$$\eta_L > \kappa_1 \eta_{ML}, \tag{13}$$

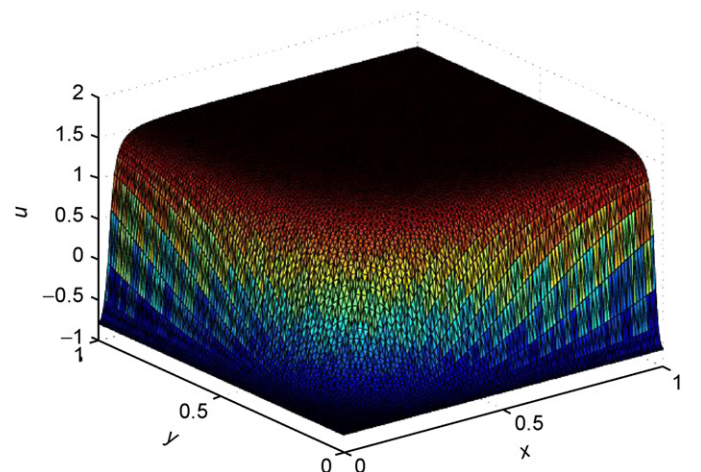


Fig. 1. Exact solution of a Poisson problem with steep gradient.

where κ_l is local refinement coefficient and η_{ML} is the maximum L2 norm of the local residual in the entire domain. Additional node will be inserted in the middle of the Delaunay cell.

The adaptation will be stop if the stopping criterion is met as

$$\nabla^2 u = \frac{2000[1 + (1000x^2y^2 - 1)^2](x^2 + y^2) - 2(2000xy)^2(x^2 + y^2)(1000x^2y^2 - 1)}{[1 + (1000x^2y^2 - 1)^2]^2}, \quad \mathbf{x} \in \Omega : [0, 1] \times [0, 1], \quad (16)$$

$$\eta_G < \kappa_g \eta_{MG}, \quad (14)$$

where κ_g is the tolerant coefficient of the estimated global residual norm and η_{MG} is the maximum estimated global residual norm throughout the adaptation process.

5. Numerical examples

In this works, numbers of numerical examples are given to demonstrate the robustness of the present error estimator and the excellence performance of the simple adaptive strategy. Adaptive analysis using different numerical methods, i.e., FEM and meshfree method are demonstrated. Comparison between the conventional residual based error estimator and the present error estimator is illustrated as well. The error norm used in this paper is defined as follows:

$$e_n = \sqrt{\frac{\sum (u^h - u^e)^2}{\sum (u^e)^2}}, \quad (15)$$

where u^h is the approximated solution and u^e is the exact solution.

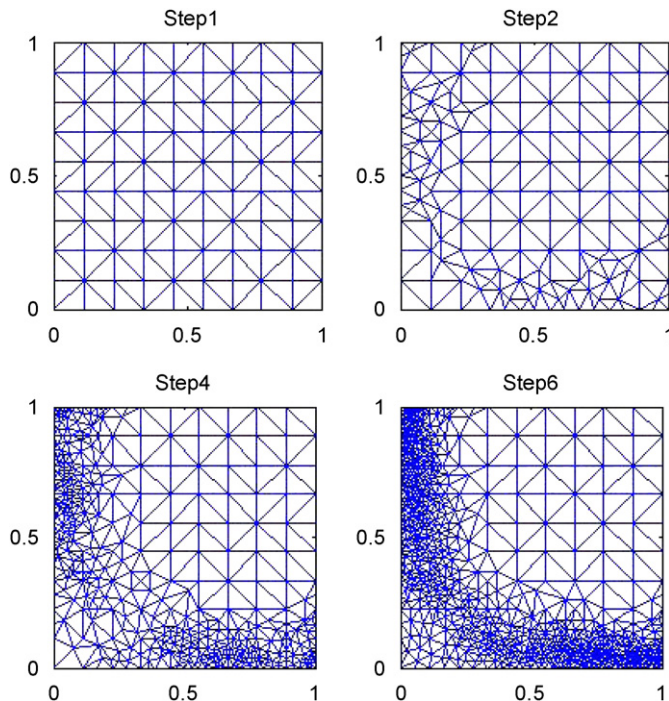


Fig. 2. Meshes at first, second, fourth and final steps.

5.1. Example 1

The first numerical example is a Poisson’s problem with a steep gradient solution. An adaptive analysis of FEM using linear triangular element is studied for the following Poisson’s equation:

with Neumann boundary conditions

$$\frac{\partial u}{\partial x} = \frac{2000xy^2}{1 + (1000x^2y^2 - 1)^2}, \quad \mathbf{x} \in \Gamma_n : x = 1,$$

and

$$\frac{\partial u}{\partial y} = \frac{2000x^2y}{1 + (1000x^2y^2 - 1)^2}, \quad \mathbf{x} \in \Gamma_n : y = 1. \quad (17)$$

And Dirichlet boundary conditions are given as

$$u = \tan^{-1}(-1), \quad \mathbf{x} \in \Gamma_u : x = 0 \quad \text{and} \quad y = 0. \quad (18)$$

The exact solution of this problem is known as

$$u = \tan^{-1}(1000x^2y^2 - 1). \quad (19)$$

The three-dimensional plot of the exact solution is shown in Fig. 1. Steep gradient exists in the solution can be observed.

In this example, the local refinement criteria and the global residual tolerance are set as $\kappa_l = 0.05$ and $\kappa_g = 0.05$. Sixteen nodes are used for constructing the RPIM shape function. The adaptation takes six steps to complete from a regularly nodal distribution with 100 nodes at initial step. The meshes at first, second, fourth and final step are shown in the Fig. 2. From the mesh of the final step, it is obvious that the region with high gradient has been refined as shown in Fig. 3. The estimated global

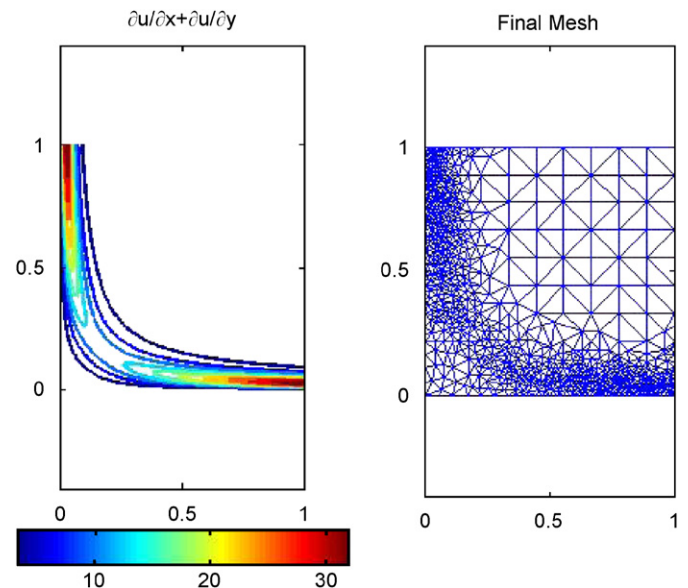


Fig. 3. Contour plot of the gradient of field function and the mesh at the final step.

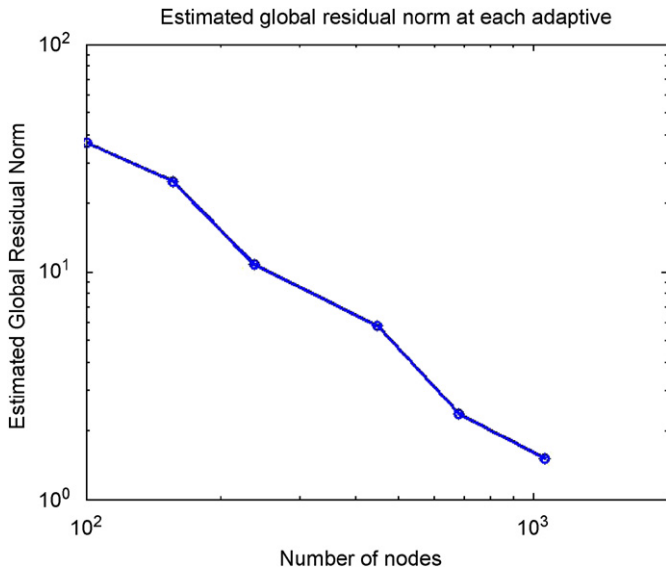


Fig. 4. Estimated global residual norm at each adaptive step.

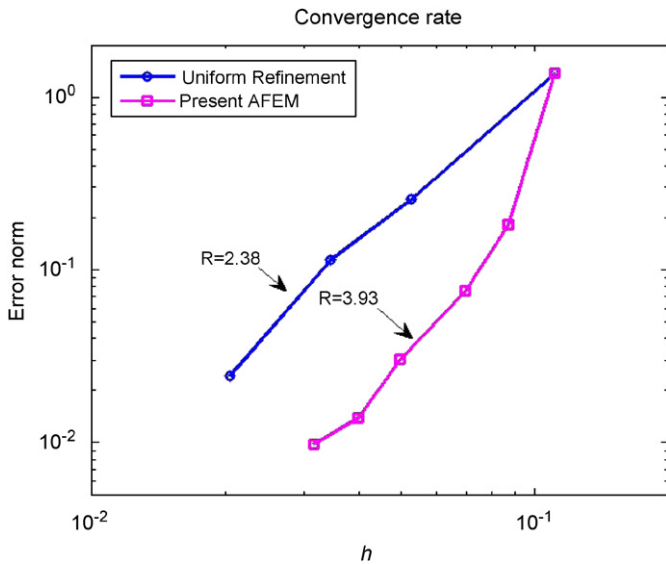


Fig. 5. Convergent rate of the solution for uniform refinement and present adaptive analysis.

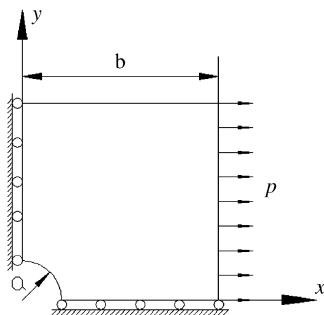


Fig. 6. Model of a quarter of infinite plate with hole.

residual norm has been reduced gradually at each adaptive, see Fig. 4. For reference purpose, the accuracy of the adaptive analysis is compared with the uniform refinement

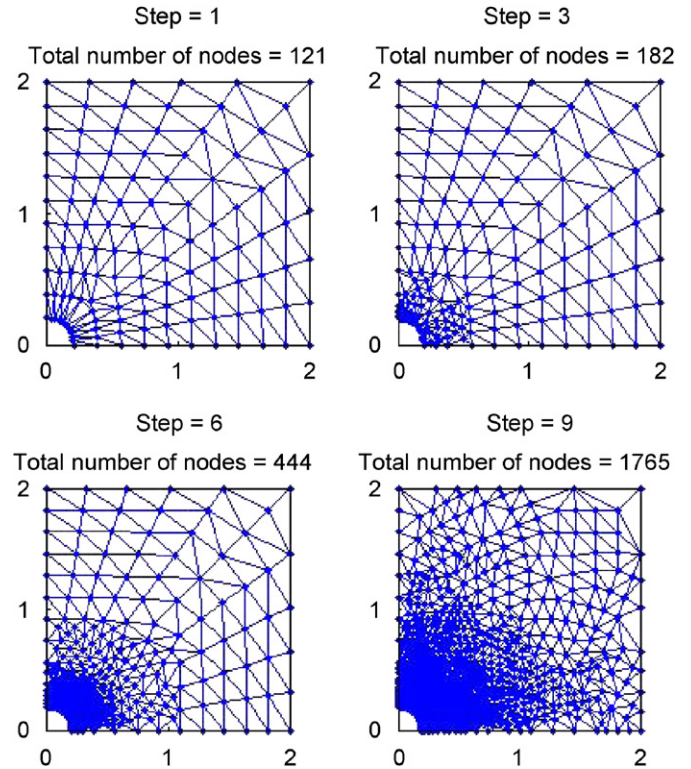


Fig. 7. Meshes at first, third, sixth and final of the adaptive step.

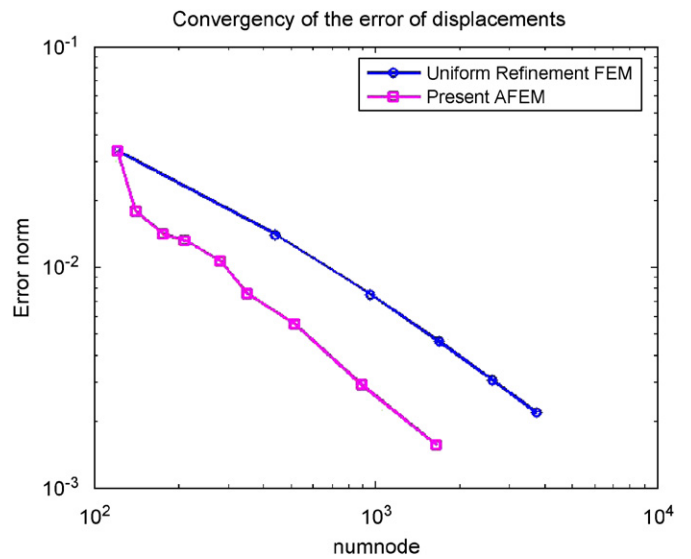


Fig. 8. Convergence of the error norm of displacements.

scheme in Fig. 5. The convergent rate of the error of our adaptive scheme is much higher than the uniform refinement scheme. This example clearly exhibits the motivation of the adaptive analysis. And the present error estimator is shown robust and effective for high gradient field function in this example.

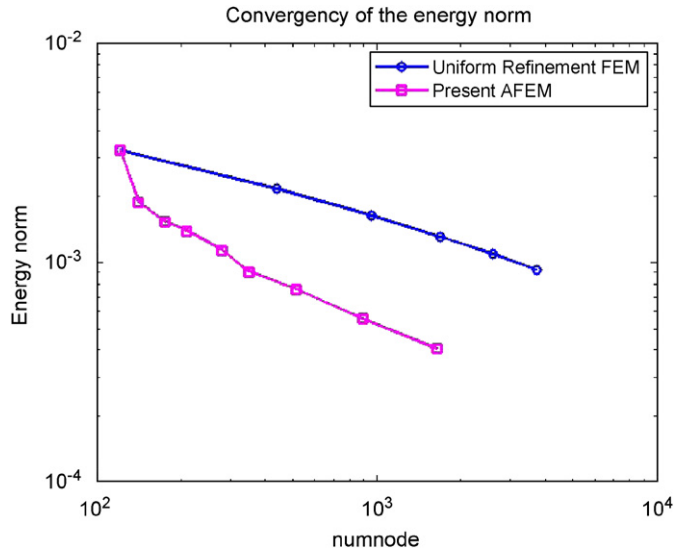


Fig. 9. Convergence of the energy norm.

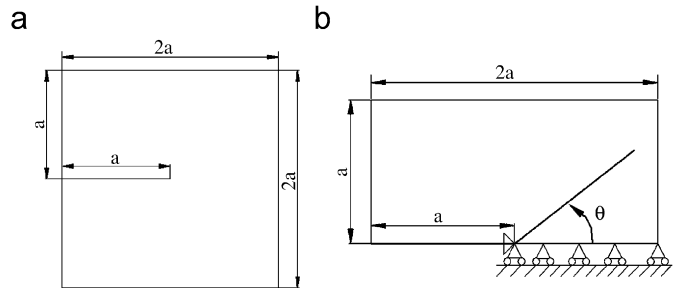


Fig. 10. (a) Full model and (b) half model of the crack panel.

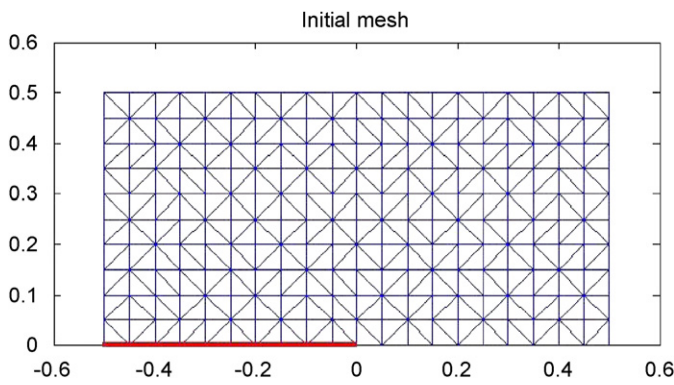


Fig. 11. Initial mesh of the adaptive analysis of the crack panel.

5.2. Example 2

A benchmark elastostatics problem is studied in example 2. An infinite plate with hole subjected to a uniaxial traction in the x -direction is considered as a plane strain problem here. The dimension and material properties are given as $b = 2.0$ m and $a = 0.2$ m, Young's modulus $E = 1 \times 10^3$ and Poisson's ratio $\nu = 0.3$. Due to symmetric, only a quarter of the plate is analysed, see Fig. 6.

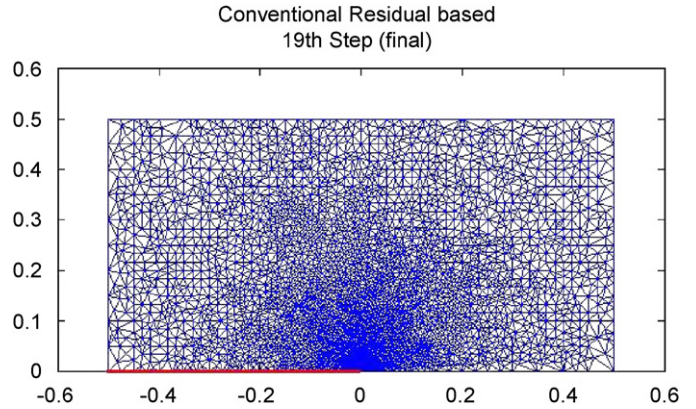


Fig. 12. Final step of the adaptive analysis using conventional residual based estimator.

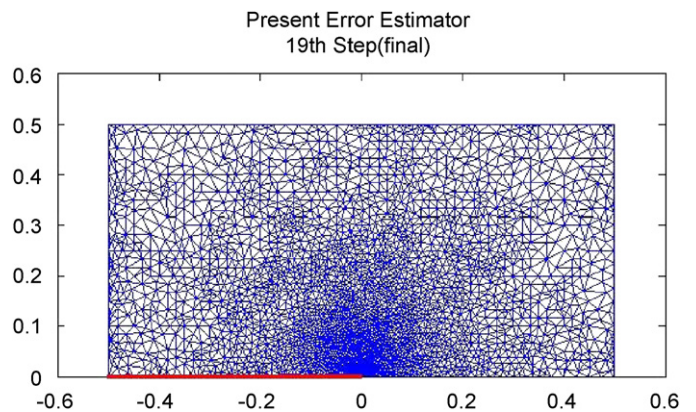


Fig. 13. Final step of the adaptive analysis using present estimator.

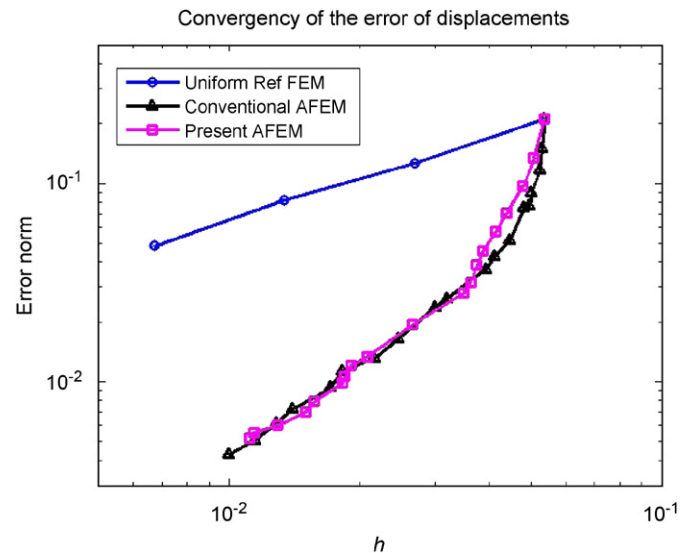


Fig. 14. Comparison of the convergence of the error norm of displacements.

The governing equation of the elastostatics problem is well known as

$$\sigma_{ij,j} + f_i = 0 \quad \text{in } \Omega. \tag{20}$$

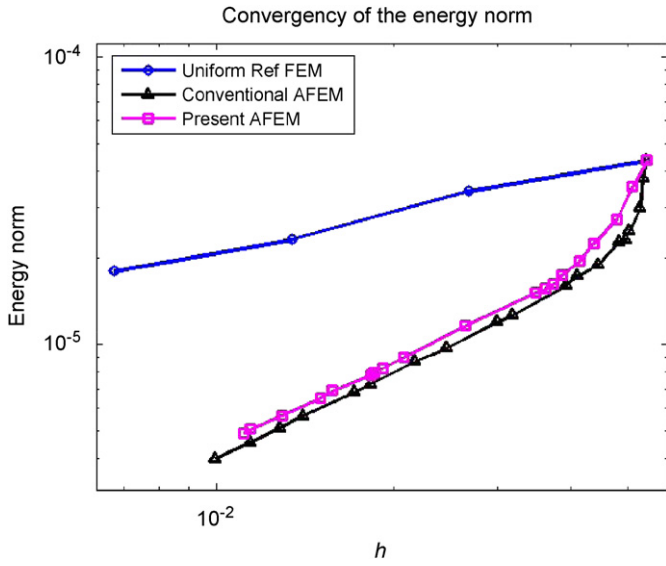


Fig. 15. Comparison of the convergence of the energy norm.

The Neumann boundary conditions are given as

$$\sigma_{ij}n_j = t_i \quad \text{along the } \Gamma_t. \quad (21)$$

And Dirichlet boundary conditions are known as

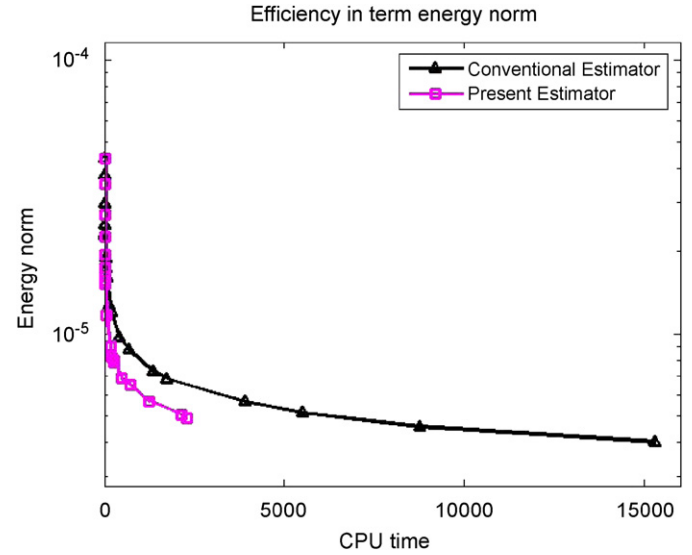
$$u_i = \bar{u}_i \quad \text{along the } \Gamma_u. \quad (22)$$


Fig. 17. Comparison of the efficiency of the error estimators in term of energy norm.

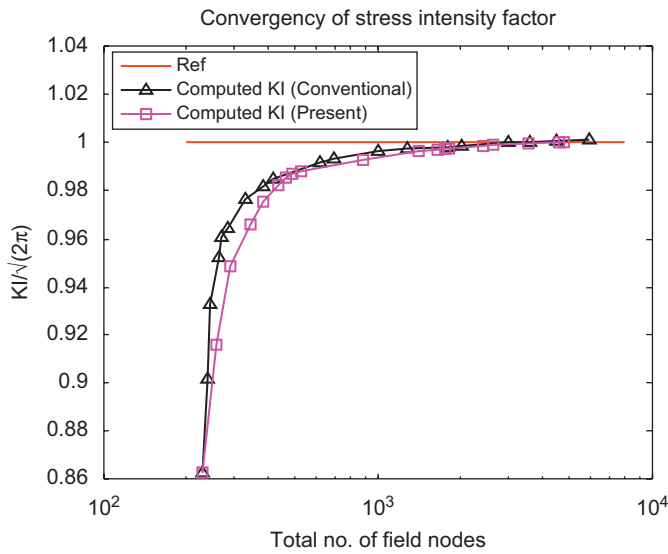


Fig. 16. Comparison of the convergence of the stress intensity factor.

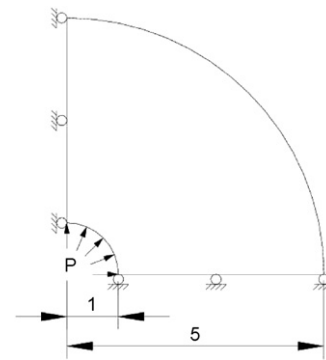


Fig. 18. Model of a quarter of cylinder subjected to an internal pressure.

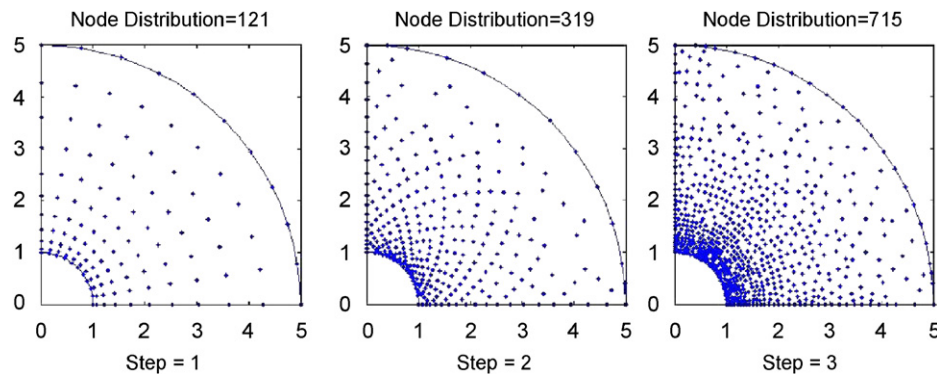


Fig. 19. Model of a quarter of cylinder subjected to an internal pressure.

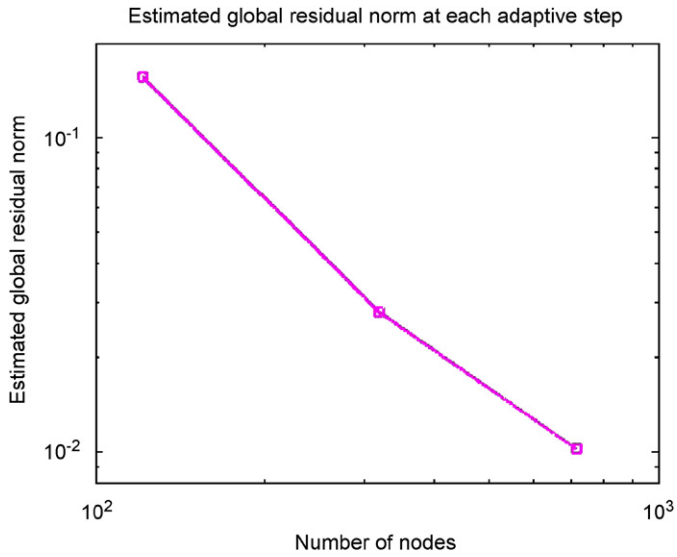


Fig. 20. Estimated residual norm at each adaptive step.

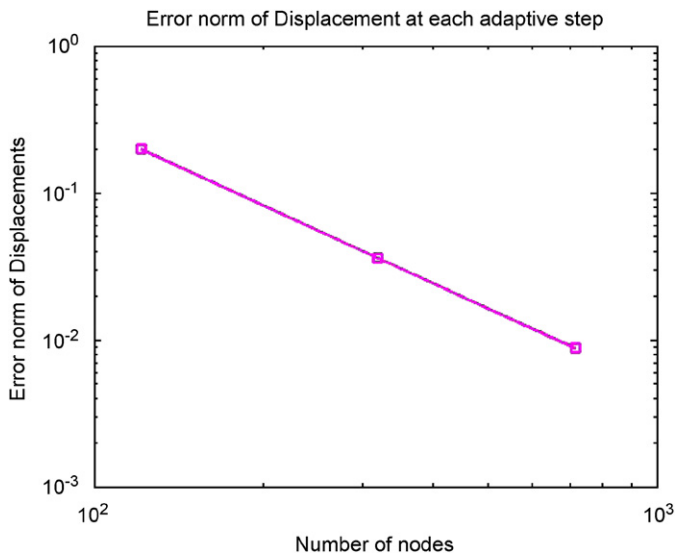


Fig. 21. Error norm of displacements at each adaptive step.

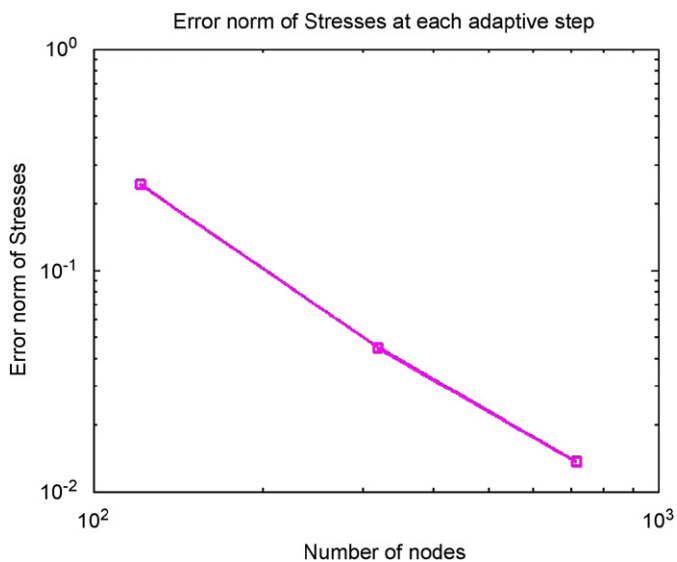


Fig. 22. Error norm of stresses at each adaptive step.

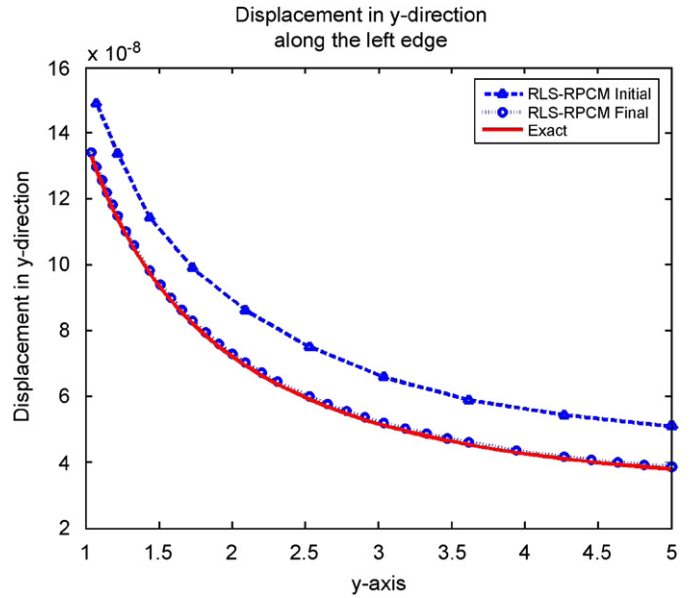


Fig. 23. The displacements in y-direction along the left edge at initial and final steps.

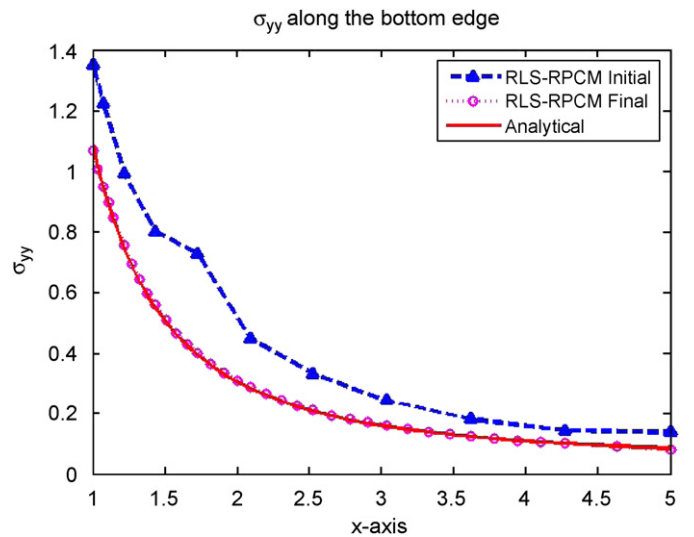


Fig. 24. The normal stress σ_{yy} along the bottom edge at initial and final step.

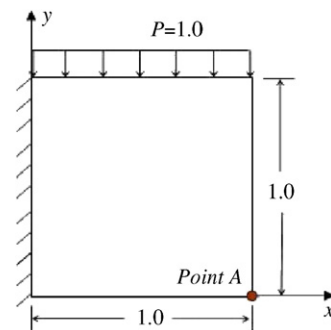


Fig. 25. Model of short beam.

In this problem, the symmetric conditions are applied along the left and the bottom edges of the model and analytical tractions are applied along the rest of the edges.

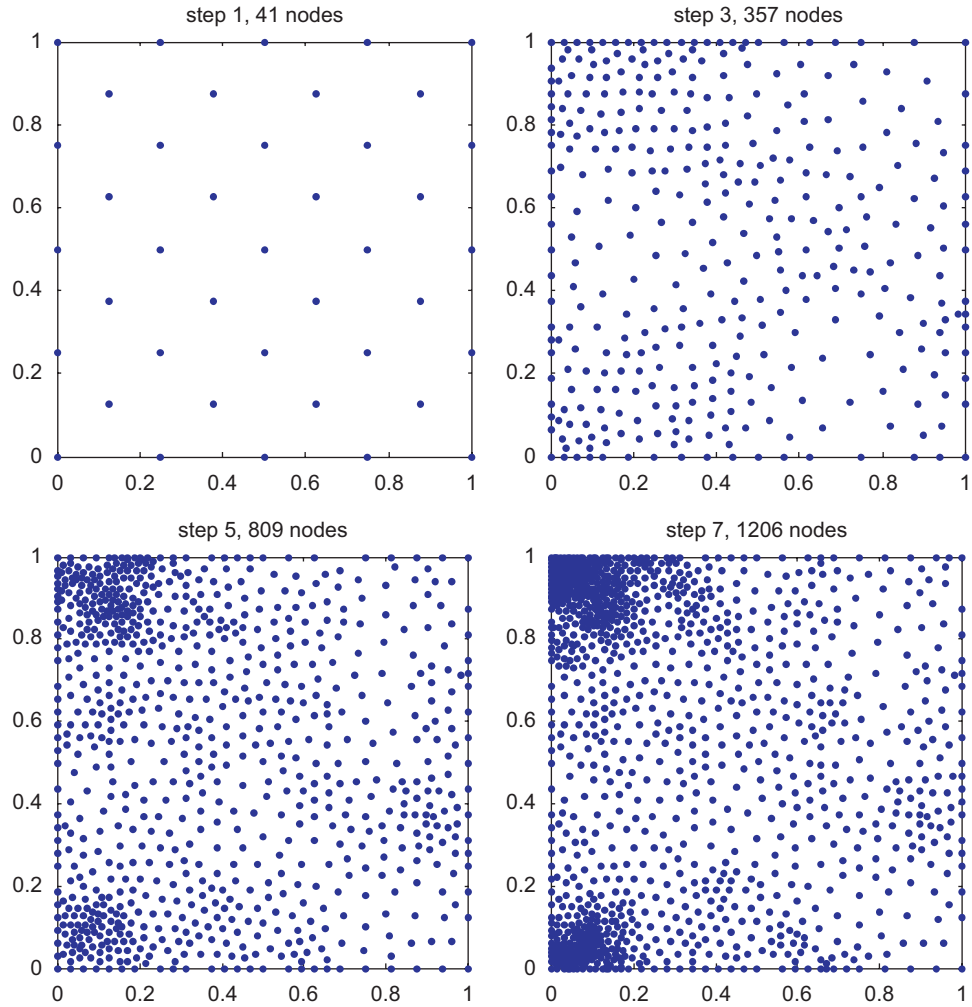


Fig. 26. Node distributions at first, third, fifth and final steps.

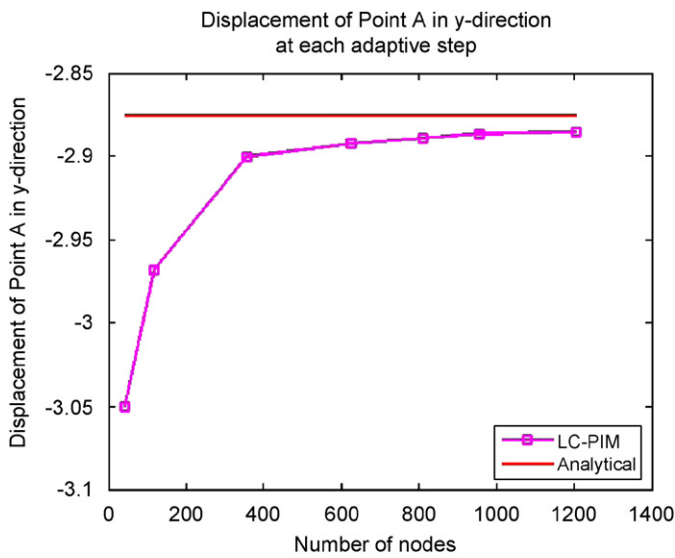


Fig. 27. The displacement of point A at each adaptive step.

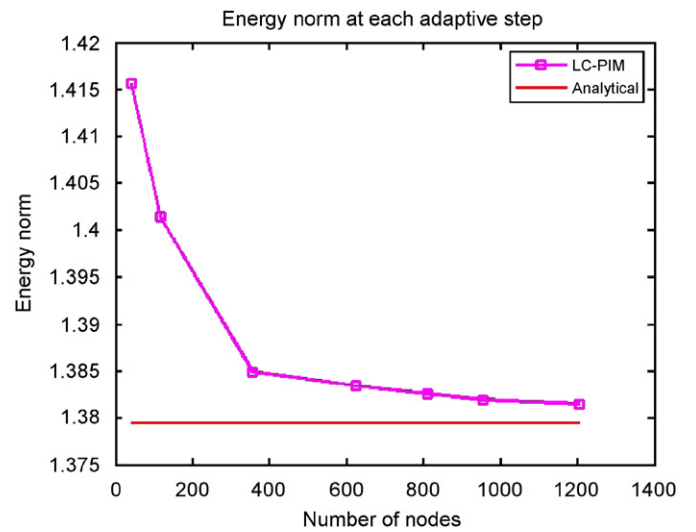


Fig. 28. The approximated energy at each adaptive step.

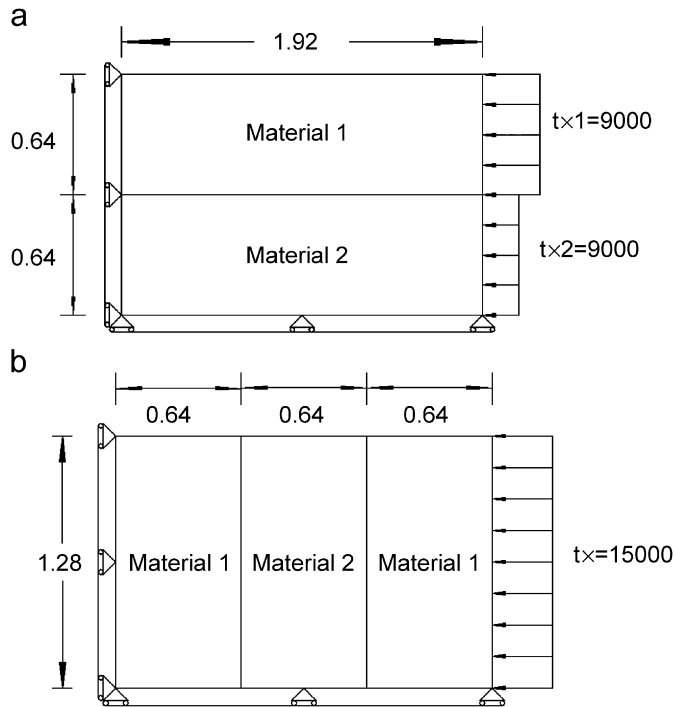


Fig. 29. (a) A panel formed by two horizontal layer and (b) a panel formed by three vertical layers.

The analytical solution of this problem can be found in [24].

The FEM with linear triangular element is used in this adaptive analysis. The local refinement coefficient and global residual tolerance are preset as $\kappa_l = 0.1$ and $\kappa_s = 0.01$, respectively. The adaptation takes nine steps to complete. The mesh at first, third, sixth and final steps are given in Fig. 7. From the meshes distribution of the final step, we can notice that the region where the stresses are concentrated is refined the most.

For comparison, this problem is studied using uniform refinement scheme as well. From the numerical solutions of the displacements and energy norm, we observed that the proposed error estimator with simple h -refinement scheme is able to provide a better convergent rate than the uniform refinement scheme as shown Figs. 8 and 9. The accuracy of the numerical solution is efficiently improved through our adaptive approach. The present error estimator has demonstrated its excellence performance to identify region where the stresses are concentrated and hence leads the simple refinement scheme to achieve a better discretization for analysis using FEM.

5.3. Example 3

In this example, a crack panel shown in Fig. 10 is considered. This problem is now considered as a plane strain problem and the material properties are known as Poisson's ratio $\nu = 0.3$, Young's modulus $E = 3 \times 10^7$. The dimension of the cracked panel is given in Fig. 10, where $a = 0.5$ m.

The cracked panel is subjected to a load along the boundaries which described as

$$\sigma_{xx} = \frac{K_I}{\sqrt{2\pi r}} \cos \frac{\theta}{2} \left(1 - \sin \frac{\theta}{2} \sin \frac{3\theta}{2} \right), \quad (23)$$

$$\sigma_{yy} = \frac{K_I}{\sqrt{2\pi r}} \cos \frac{\theta}{2} \left(1 + \sin \frac{\theta}{2} \sin \frac{3\theta}{2} \right), \quad (24)$$

$$\tau_{xy} = \frac{K_I}{\sqrt{2\pi r}} \sin \frac{\theta}{2} \cos \frac{\theta}{2} \cos \frac{3\theta}{2}, \quad (25)$$

where K_I is stress intensity of mode I . Due to symmetric, only half of the model is analysed, see Fig. 10(b).

In this example, the adaptive analyses of FEM using both conventional residual based error estimator and the present error estimator that using RBFs are studied. The initial mesh for FEM is given in Fig. 11. Linear triangular element is used in the FEM.

The conventional residual based error estimator is adopted from Babuska [20] as

$$\eta_L = \sqrt{|T|^2 (\Pi_T \mathbf{f})^2 + \frac{1}{2} \sum_{\ell \in E_T} |\ell|^2 \mathbf{J}_\ell^2} \quad (26)$$

where triangle element $T \in T_h$, E_T is the edges of the element T , and

$$\Pi_T \mathbf{f} := \frac{1}{|T|} \cdot \int_T \mathbf{f} \, d\Omega. \quad (27)$$

For each edge ℓ of the element, \mathbf{J}_ℓ is the traction jump along the element interface.

The final mesh of the adaptive analysis using both conventional and present error estimator are shown in Figs. 12 and 13, respectively. From the final mesh given in Figs. 12 and 13, we notice that the distributions of the meshes of the FEM using two different estimators are very similar. The present error estimator using RBFs is able to identify the singularity point at the crack tip and leads the refinement scheme effectively to achieve a better discretization mesh during the adaptive analysis.

From the error norms of displacement and energy norm, both estimators provide excellent performance as shown in Figs. 14 and 15. A uniform refinement scheme is also carry out to compare with the adaptive analyses using both error estimators. From both Figs. 14 and 15, the motivation of the adaptive analysis is clearly demonstrated. Better accuracy can be achieved by the adaptive analysis using both error estimators with less amount of mesh compared to uniform refinement scheme. Convergency of the stress intensity factor at each adaptive step computed using both error estimators also plotted in Fig. 16 for reference purpose. The performance of present error estimator is as good as the conventional residual based error estimator. To compare the cost effectiveness between two estimators, the present error estimator is found more cost effective than the conventional estimator as shown in Fig. 17. It is because the procedure of measuring the traction jump along the interface between element cost more that the direct integration of the residual in the local domain. The direct integration using one

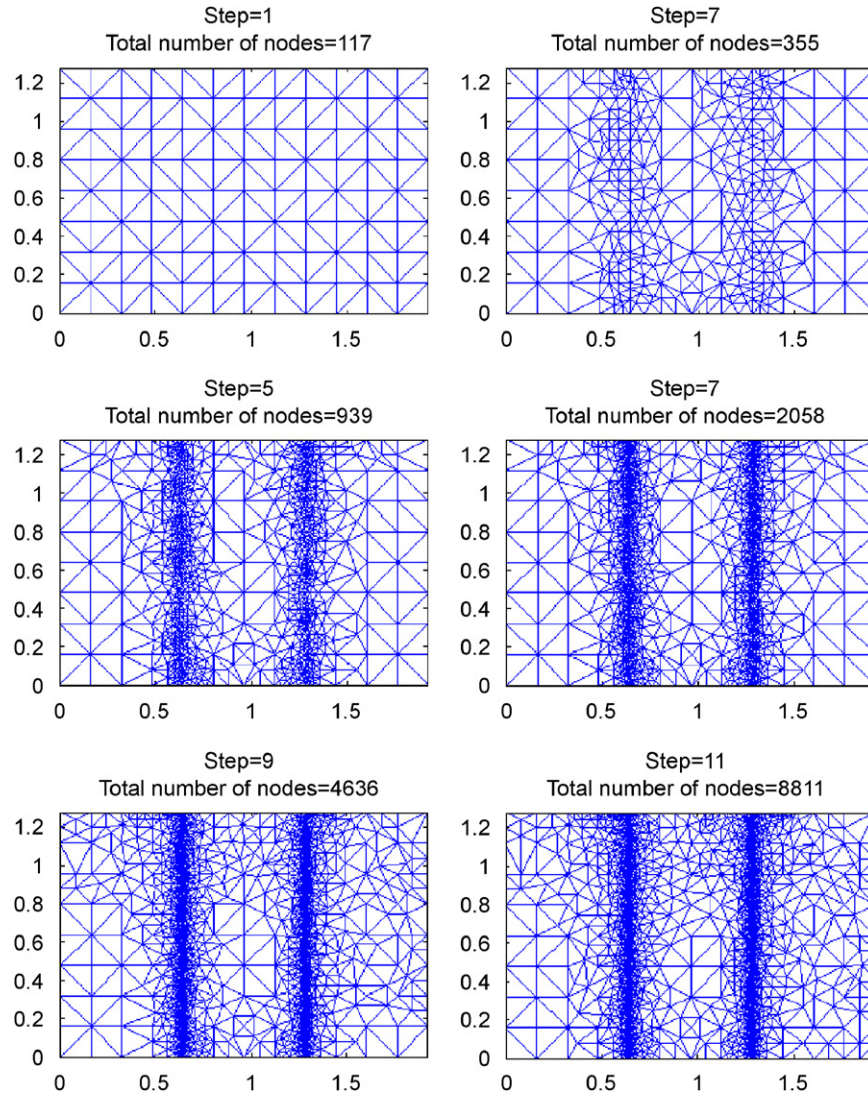


Fig. 30. Meshes at first, third, fifth, seventh, ninth and final steps.

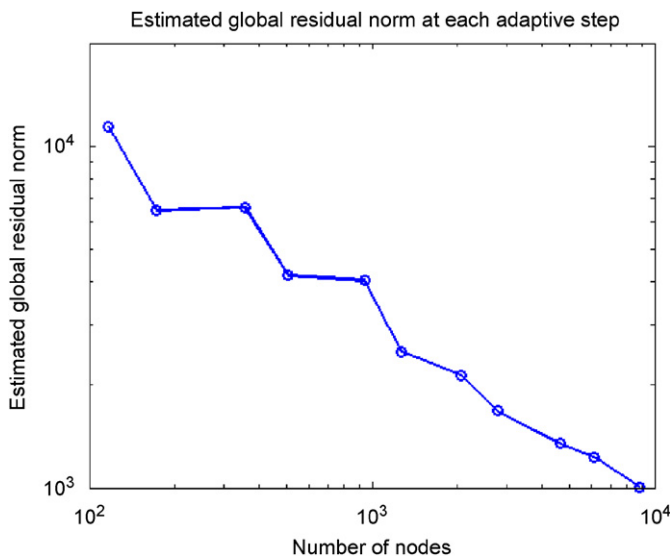


Fig. 31. Estimated global residual norm at each adaptive step.

gauss point is shown robust, effective and reliable to evaluate the present error estimator.

5.4. Example 4

In this example, the present error estimator is used in the adaptive meshfree strong-form method. The strong-form method is a truly mesh free method as it is formulated without any mesh. Therefore, the recovery based error estimator that relies on the recovering process is not possible to be adopted to perform the adaptive meshfree strong-form method. Unlike the recovery based error, the knowledge of recovering points is not required for the present error estimator. The strong-form meshfree method can be easily adopted the present error estimator that using RBFs for performing adaptive analysis. In this works, the regularized least-squares radial point collocation method (RLS-RPCM) is used in this adaptive analysis. The detailed formulation of the RLS-RPCM can be found in [18].

A cylinder subjected to an internal pressure is analysed in this example. Due to the symmetric, only a quarter of the cylinder is modelled. The dimension of the cylinder is given in Fig. 18. The material properties is given as Poisson’s ratio $\nu = 0.3$ and Young’s modulus $E = 1 \times 10^7$. The internal pressure is known as $P = 1$.

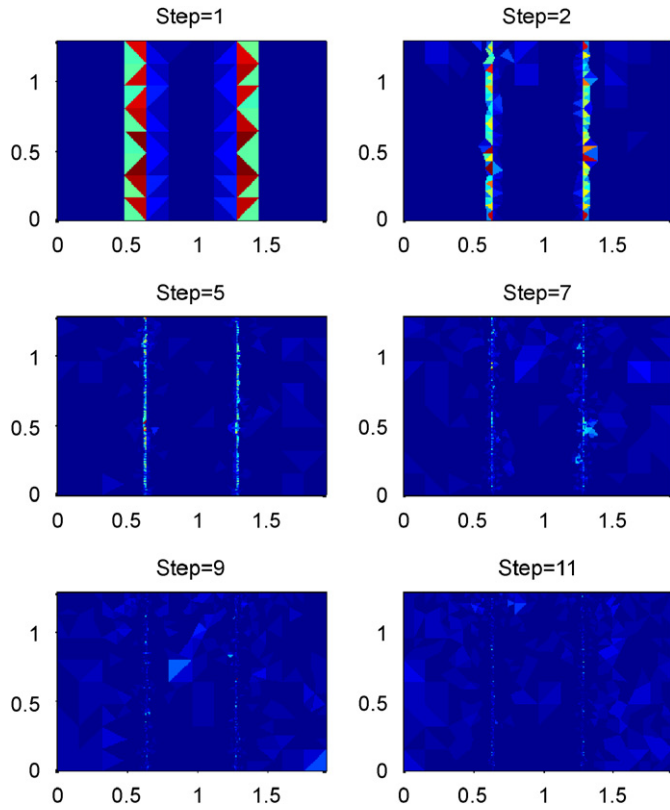


Fig. 32. Estimated residual at first, third, fifth , seventh, ninth and final steps.

The local refinement coefficient and global residual tolerance are predefined as $\kappa_l = 0.05$ and $\kappa_g = 0.1$, respectively. The adaptive analysis started with 121 nodes in the domain and takes three steps to complete with 715 nodes, see Fig. 19. The estimated global residual norm is gradually reduced in the adaptive process as shown in Fig. 20. Additional nodes are added according to the present error estimator using RBFs. The accuracy of the displacements and stresses are greatly improved as shown in Figs. 21 and 22. From the displacements in y -direction along the left edge and the normal stress σ_{yy} along the bottom edge are plotted at initial and final step, tremendous improvement of the numerical solution is observed (Figs. 23 and 24).

From this example, the residual based error estimator using RBFs is again shown appropriate for implemented in strong-form adaptive analysis. Excellence performance of the present error estimator is exhibited while the recovery based error estimator is not possible to be used here.

5.5. Example 5

Example 5 is an adaptive meshfree weak-form method [25]. A short cantilever beam subject to a uniform loading on the top edge is studied and considered as a plane strain problem here. The dimension of the short beam is indicated in Fig. 25 and the material properties are known as: Young’s modulus $E = 1.0$ and Poisson’s ratio $\nu = 0.3$. Loading applied on the top edge is given as $P = 1.0$. The similar problem is also studied in [9] as well.

As the exact solution is not available, a reference solution computed by FEM with very fine mesh of 58 060 degree of freedom is considered as an ‘analytical’ solution. The displacement in y -direction of point A is -2.875323 and the energy norm is given as $\|u\| = 1.3794663$.

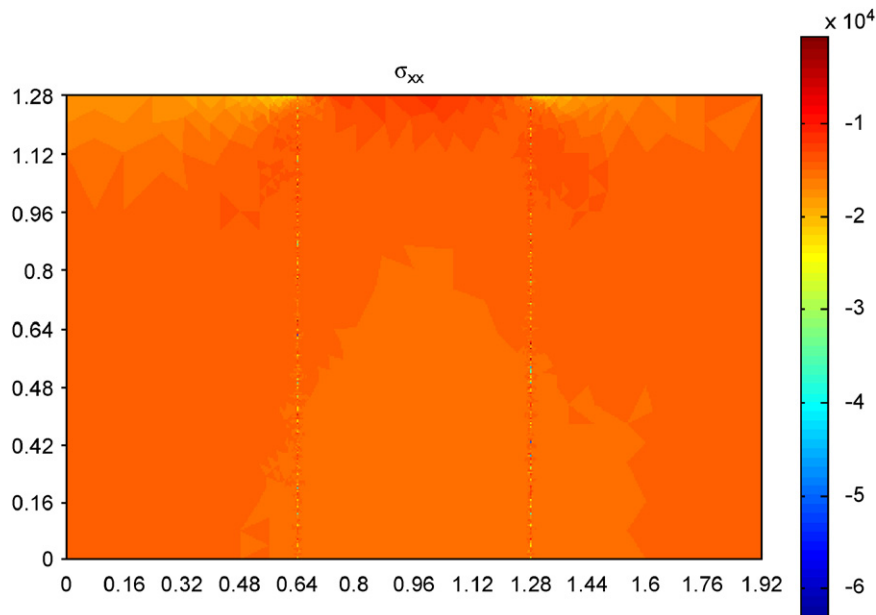


Fig. 33. Distribution of normal stress σ_{xx} at final step.

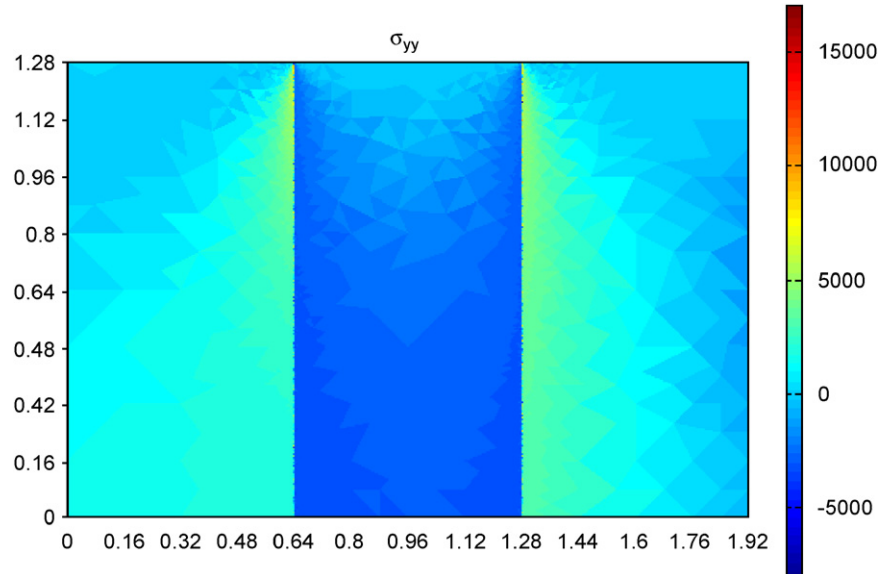


Fig. 34. Distribution of normal stress σ_{yy} at final step.

Since there are two singularity points exist at the two corner of the beam near to the wall, the meshes around singularity points are expected to be refined. In this example, the local refinement coefficient is predefined as $\kappa_1 = 0.05$ and global residual tolerance is set as $\kappa_g = 0.2$. The adaptive analysis takes seven steps to completed. Node distributions at initial, third, fifth and final step are plotted in Fig. 26. From the final distribution, the proposed error estimator has demonstrated its robustness of identifying the all singularity points exist in the problem domain. More additional nodes have been inserted around the singularity points.

From this example, we can observe that the proposed error estimator is able to identify the singularity points. The region near to the singularity points has to be refined in order to improve the accuracy of the numerical solution. Accuracies of the displacement and energy norm are also against the reference solution that are plotted in Figs. 27 and 28.

It is evidently clear that the present error estimator is also feasible for meshfree weak-form method to perform adaptive analysis. The error estimator using RBFs is robust and able to lead the refinement scheme to refine the region where singularity points exist.

5.6. Example 6

In this example, a heterogeneous panel with unit thickness subjected to a compression load in horizontal direction is considered as shown in Fig. 29(a). This panel consists of two different materials and is made up by two horizontal layers. The material properties are given as Young's modulus: $E_{\text{mat}1} = 3 \times 10^5$, $E_{\text{mat}2} = 3 \times 10^4$ and Poisson's ratio: $\nu_{\text{mat}1} = \nu_{\text{mat}2} = 0.25$.

Two different compression loads are applied to the left edge of the panel as shown in Fig. 29(a), where $t_{x1} = 9000$, $t_{x2} = 900$. Such loading configuration results in a constant strain and linear

displacement field function over the entire domain. The strain is known as $\varepsilon_x = 0.30$ and exact solution of displacements are known as $u_x = 3 \times 10^{-2}x$ and $u_y = -0.75 \times 10^{-2}x$.

As linear displacements field can be reproduced by the linear triangle element in FEM, the solution of the FEM is same as the exact solution. Similarly, the RPIM shape functions using in the present error estimator is able to reproduce linear function. Hence, the present error estimator effectively shows no error exists in the finite element solution. In the paper of Sydenstriker et al. [26], numerical example had shown that the error estimators given by Zienkiewicz et al. [1,27] indicate error that does not exist in the problem domain across the interface of the two layers.

5.7. Example 7

In Example 7, another heterogeneous panel with unit thickness subjected to a compression load in horizontal direction is considered as shown in Fig. 29(b). This panel consists of two different materials and is made up by three vertical layers. The material properties are given as Young's modulus: $E_{\text{mat}1} = 3 \times 10^5$, $E_{\text{mat}2} = 3 \times 10^4$ and Poisson's ratio: $\nu_{\text{mat}1} = \nu_{\text{mat}2} = 0.25$.

In this case, a constant compression load is applied to the left edge of the panel as shown in Fig. 29(b), where $t = 15000$. Such loading configuration results in a discontinuous stress distribution. Large error is expected to be found along the interfaces between layers.

An adaptive analysis is conducted in this example. The local refinement coefficient is predefined as $\kappa_1 = 0.05$ and global residual tolerance is set as $\kappa_g = 0.1$. The adaptive analysis takes 11 steps to complete. Node distributions at initial, third, fifth and final step are plotted in Fig. 30. From the final distribution, it is clear that most of the nodes are inserted along the interfaces between two differences layer of material due to the

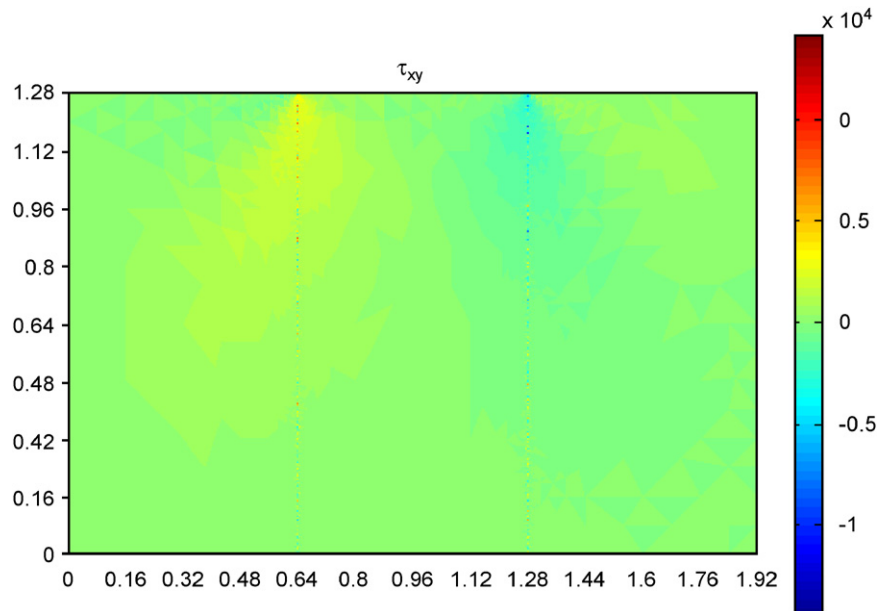


Fig. 35. Distribution of shear stress τ_{xy} at final step.

discontinuous of the stress field. The present error estimator has effectively identified the error along the interfaces as shown in Fig. 31. From the estimated global residual norm given in Fig. 32, the norm has been reduced gradually till the end of the adaptive analysis. Normal stresses and shear stress distributions are given in Figs. 33–35 for reference purpose.

From this example, it is clear that the present residual error estimator is versatile and also feasible for heterogeneous material in adaptive analysis.

6. Conclusion

In this paper, a very simple residual based error estimator using radial basis functions (RBFs) is present. The present error estimator has shown simple, robust and versatile. From the numerous examples, excellence performance of the present error estimator is observed. The present error estimator is able to reflect the local error and leads the adaptation to a better discretization with simple refinement scheme. We have also shown the present error estimator is suitable for various kinds of numerical method. The present error estimator is not only feasible for numerical method that formulated relying on mesh, such as finite element method, but also applicable to the mesh-free method. Furthermore, regardless of formulation procedure, the present error estimator is feasible for both weak and strong form method. In addition, the present error estimator also shown good performance for problems dealing with heterogeneous materials Without much modification, such simple error estimator can be easily embraced in the existing code of numerical method to perform the adaptive analysis. Compared to recovery based and conventional residual based error estimator, the present error estimator has been shown very more versatile, simple and easy to implement in adaptive analysis.

At this stage of development, the present error estimator is restricted for linear problems with homogenous material only. In the future development, the proposed residual error estimator is potentially extended for nonlinear problems.

References

- [1] O.C. Zienkiewicz, J.Z. Zhu, A simple error estimator and adaptive procedure for practical engineering analysis, *Int. J. Numer. Methods Eng.* 24 (1987) 337–357.
- [2] N.E. Wiberg, F. Abdulwahab, Patch recovery based on the superconvergent derivatives and equilibrium, *Int. J. Numer. Methods Eng.* 36 (1993) 2703–2724.
- [3] N.E. Wiberg, F. Abdulwahab, S. Ziukas, Enhanced superconvergent patch recovery incorporating equilibrium and boundary conditions, *Int. J. Numer. Methods Eng.* 37 (1994) 3147–3440.
- [4] T. Blacker, T. Belytschko, Superconvergent patch recovery with equilibrium and conjoint interpolant enhancements, *Int. J. Numer. Methods Eng.* 37 (1994) 517–536.
- [5] O.C. Zienkiewicz, J.Z. Zhu, The superconvergent patch recovery and a posteriori error estimates. Part 1: the recovery technique, *Int. J. Numer. Methods Eng.* 33 (1992) 1331–1364.
- [6] O.C. Zienkiewicz, J.Z. Zhu, The superconvergent patch recovery and a posteriori error estimates. Part 2: error estimates and adaptivity, *Int. J. Numer. Methods Eng.* 33 (1992) 1365–1382.
- [7] O.C. Zienkiewicz, J.Z. Zhu, The superconvergent patch recovery and adaptive finite element refinement, *Comput. Methods Appl. Mech. Eng.* 101 (1992) 207–224.
- [8] I. Babuska, W.C. Rheinboldt, A posteriori error estimates for the finite element method, *Int. J. Numer. Methods Eng.* 12 (1978) 1597–1615.
- [9] M. Ainsworth, J.T. Oden, A unified approach to a posteriori error estimation using element residual methods, *Numer. Math.* 65 (1993) 23–50.
- [10] R. Franke, Scattered data interpolation: test of some methods, *Math. Comput.* 38 (157) (1982) 181–200.
- [11] H. Wendland, Piecewise polynomial, positive definite and compactly supported radial basis functions of minimal degree, *Adv. Comput. Math.* 4 (1995) 389–396.

- [12] E.J. Kansa, Multiquadrics-a scattered data approximation scheme with applications to computational fluid-dynamics I&II, *Comput. Math. Appl.* 19 (8/9) (1990) 127–161.
- [13] E.J. Kansa, Y.C. Hon, Circumventing the ill-conditioning problem with multiquadric radial basis functions: application to elliptic partial differential equations, *Comput. Math. Appl.* 39 (2000) 123–137.
- [14] G.R. Liu, Y.T. Gu, A local radial point interpolation method (LRPIM) for free vibration analyses of 2-D solids, *J. Sound Vibr.* 246 (1) (2001) 29–46.
- [15] G.R. Liu, G.Y. Zhang, Y.T. Gu, Y.Y. Wang, A meshfree radial interpolation method for three-dimensional solid problem, *Comput. Mech.* 36 (2005) 421–430.
- [16] J.G. Wang, G.R. Liu, On the optimal shape parameters of radial basis function, *Comput. Methods Appl. Mech. Eng.* 191 (2002) 21–26.
- [17] X. Liu, G.R. Liu, K. Tai, K.Y. Lam, Radial basis interpolation collocation method for the solution of partial differential equations, *Comput. Math. Appl.* 50 (2005) 1425–1442.
- [18] B. Bernard, T. Kee, G.R. Liu, C. Lu, A regularized least-squares radial point collocation method (RLS-RPCM) for adaptive analysis, *Comput. Mech.* 40 (5) (2007) 837–853.
- [19] G.R. Liu, Y.T. Gu, A matrix triangulation algorithm for the point interpolation method, *Comput. Methods Appl. Mech. Eng.* 192 (19) (2003) 2269–2295.
- [20] I. Babuska, R. Duran, R. Rodriguez, Analysis of the efficiency of an a posteriori error estimator for linear triangular finite element, *SIAM J. Numer. An.* 29 (4) (1992) 947–964.
- [21] G.R. Liu, *Meshfree Method: Moving Beyond the Finite Element Method*, CRC Press, 2002.
- [22] G.R. Liu, Y.T. Gu, *An Introduction to Meshfree Methods and Their Programming*, Springer, Berlin, 2003.
- [23] R.L. Hardy, Theory and applications of multiquadrics-biharmonic method (20 years of discovery 1968–1988), *Comput. Math. Appl.* 19 (8/9) (1990) 163–208.
- [24] S.P. Timoshenko, J.N. Goodier, *Theory of Elasticity*, McGraw-Hill, New York, 1970.
- [25] G.R. Liu, G. Y. Zhang, Y.T. Gu, Y.Y. Wang, A linearly conforming point interpolation method (LC-PIM) for 2D solid mechanics problems, *Int. J. Comput. Methods* 2 (4) (2005) 645–665.
- [26] R.M. Sydenstricker, A. Coutinho, M. Martins, L. Landau, J. Alves, A posteriori error estimate for stress analysis of homogeneous and heterogeneous materials: an engineering approach, *Finite Elem. Anal. Des.* 42 (2005) 171–188.
- [27] O.C. Zienkiewicz, R.L. Taylor, *The finite element method*, McGraw-Hill, London, 1989.